

ARTICLE OPEN



Amplifying subtropical hydrological transition over China in early summer tied to weakened mid-latitude synoptic disturbances

Yana Li¹✉, Yi Deng², Ho-Nam Cheung^{3,4}, Wen Zhou^{1,5}✉, Song Yang^{3,4} and Henian Zhang²

The rainy season over southern China (SC) begins with the onset of the South China Sea monsoon around mid-May. We demonstrate here that the SC precipitation exhibits a notable drying (wetting) trend prior to (after) the monsoon onset, leading to a more abrupt thus amplified hydrological transition over SC in early summer. The contrasting precipitation trends are largely driven by the recent decline in mid-latitude synoptic eddy activity. Weakened mid-latitude synoptic disturbances suppress SC frontal activities before the monsoon onset, facilitating the drying trend, and enhance the spatial stationarity of the SC monsoonal front after the monsoon onset, leading to the wetting trend. CMIP6 models in general fail to capture the contrasting trends between the two periods. In models where both the trends in precipitation and mid-latitude synoptic eddy activity are well captured, the amplification of the hydrological transition over SC is projected to continue well into the late 21st century. Our results highlight the footprints of hemispheric-scale climate change in regional hydroclimate and the obvious challenges faced by climate models in capturing such footprints.

npj Climate and Atmospheric Science (2022)5:40; <https://doi.org/10.1038/s41612-022-00259-1>

INTRODUCTION

Global subtropical precipitation undergoes an observed and projected decline under global warming^{1,2}, with considerable regional and temporal variability^{3,4}. The East Asian summer monsoon region is projected to have enhanced precipitation and more extreme events in the late 21st century⁵. Therefore, southern China, which includes a subtropical coastline in the East Asian monsoon region, features large variability of precipitation and is vulnerable to global warming. How the precipitation over southern China varies with climate change is an important socioeconomic issue, because southern China holds about 2/3 of the population of China, and urbanized regions such as the Pearl River Delta have been expanding in southern China as a fast-growing economic center and high-tech hub. The infrastructure inside this metropolitan area is vulnerable to high-impact weather events such as heavy precipitation and drought⁶. Policy makers and investors should be better prepared for the potential risks due to the future precipitation trend under global warming.

The rainy season in southern China ranges from April to September, the first half of which is called the pre-rainy season, i.e., April to June^{7,8}. The diabatic heating produced by such an intense rainy season is a major part of the East Asian summer monsoon heating, which affects the structure and strength of the subtropical high over the Pacific and tends to force a stationary wave pattern of global influence, for instance on the American-Atlantic regions^{9–13}. Around mid-May, the onset of the South China Sea summer monsoon (SCSSM) marks the commencement of the monsoonal rainy season^{14–16}. After the SCSSM onset, precipitation over southern China increases more than 40% as compared to that before the monsoon onset¹⁶. The precipitation

of the pre-rainy season is classified into cold frontal precipitation and summer monsoonal precipitation with respect to the SCSSM onset^{15,16}. The first type of precipitation is linked to cold fronts, which are closely associated with synoptic disturbances in the mid-latitudes^{17,18}. The second type is associated with convective instability and quasi-stationary fronts, which are the slow-moving and long-lasting East Asian summer monsoon systems, with large spatial coverage over land and ocean¹⁵. Variation in the quasi-stationary fronts is modulated mainly by the western North Pacific subtropical high, tropical sea surface temperature (SST), westerly jet streams, and atmospheric eddies from the mid-latitudes^{17–20}. Both tropical and mid-latitude forcings are thus crucial for the pre-rainy season precipitation over southern China. In this study, the pre-rainy season is divided into two periods, the pre-monsoon onset (pre-MO) and post-monsoon onset (post-MO), with respect to the SCSSM onset due to the different forcings involving precipitation.

While the SCSSM has tended to commence earlier and has intensified since the early 1990s, the summer precipitation over southern China experienced a prominent decadal strengthening in the mid-1990s^{21–25}. Besides the summer decadal trend, Zhu et al.²⁶ found an out-of-phase decadal shift in the spring and summer precipitation over southern China from 1979–1992 to 1997–2010, with drier springs and wetter summers in the latter period. They proposed that a springtime La Niña-like decadal SST anomaly pattern in the tropical Pacific could trigger more convection over the Maritime Continent and cause anomalous descending motion over southern China, while summertime decadal warming over the Indian Ocean could inhibit convection over the Maritime Continent and strengthen the monsoon trough

¹Guy Carpenter Asia-Pacific Climate Impact Center, Center for Ocean Research in Hong Kong and Macau (CORE), School of Energy and Environment, City University of Hong Kong, Hong Kong SAR, China. ²School of Earth and Atmospheric Sciences, Georgia Institute of Technology, Atlanta, GA, USA. ³School of Atmospheric Sciences and Guangdong Province Key Laboratory for Climate Change and Natural Disaster Studies, Sun Yat-sen University, Zhuhai, China. ⁴Southern Marine Science and Engineering Guangdong Laboratory (Zhuhai), Zhuhai, China. ⁵Department of Atmospheric and Oceanic Sciences, Fudan University, Shanghai, China. ✉email: yanali@cityu.edu.hk; wen_zhou@fudan.edu.cn

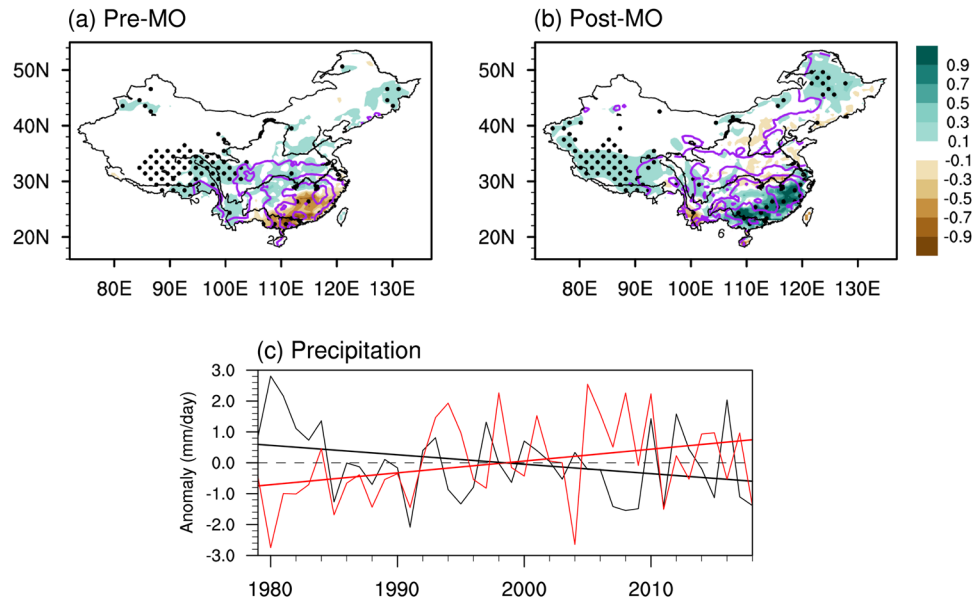


Fig. 1 Contrasting precipitation trends in early summer over southern China. Precipitation trends in **a** 1 April – 15 May (the pre-monsoon onset period (pre-MO)) and **b** 16 May – 30 June (the post-monsoon onset period (post-MO)) over China in 1979–2018 (shading, mm/day/decade). Purple contours indicate the corresponding climatology of daily precipitation in 1979–2018 (mm; referring to 2, 4, 6, and 8 mm/day from north to south). Stippled areas are significant at the 0.1 level in **a** and at the 0.05 level in **b**. **c** Time series of areal-mean precipitation anomalies (mm/day) over southern China (SC, 20–28°N/105–120°E) in the pre-MO period (black curve) and the post-MO period (red curve). Slanted solid lines are the corresponding linear regressions with coefficients of -0.31 and $+0.38$ mm/day/decade, significant at the 0.1 and 0.05 levels, respectively.

over southern China, leading to positive precipitation anomalies. In this study, we will show an opposite precipitation trend over southern China around one month before and after the SCSSM onset in mid-May, which indicates a more amplified regional hydrological seasonal transition over southern China in its pre-rainy season (Fig. 1). Because the long-term trends in SST are similar on timescales of less than three months (Supplementary Fig. 1), we will show the factors excluding the tropical SST anomalies that contribute to this opposite trend.

Northern mid-latitudes, especially over Eurasia, have experienced a weakening summer circulation in the past 40 years^{27,28}, accompanied by more persistent heat waves and droughts in recent summers^{29,30}. These changes are partly associated with declining midlatitude synoptic activity and associated low eddy kinetic energy in boreal summer^{31,32}. Although the causes of such a weakening summer circulation are still being debated, its impact on weather patterns in Eurasia is substantial and brings additional socioeconomic risk to the region^{31,33}. As mentioned previously, mid-latitude forcing is also an indispensable factor in the SCSSM onset and the summer precipitation over southern China. We will demonstrate the impact of weakened mid-latitude circulation on the out-of-phase precipitation trend over southern China in its pre-rainy season.

RESULTS

Out-of-phase precipitation trend in the pre-MO and post-MO periods

The SCSSM onset marks the transition from boreal spring to summer, when the southwesterly monsoon prevails over southern China. Climatologically, the daily precipitation over southern China increases abruptly from about 5 mm/day in April to about 8.5 mm/day in June (Supplementary Fig. 2). As illustrated in Fig. 1, southern China exhibits a significant drying trend in the pre-MO period (1 April–15 May) and a significant wetting trend in the post-MO period (16 May–30 June), suggesting an abrupt transition of the rainy season and an amplified spring-to-summer transition

of the regional hydroclimate system in recent decades. Here, we define southern China as $20\text{--}28^{\circ}\text{N}/105\text{--}120^{\circ}\text{E}$. The regional-mean precipitation time series has a robust long-term trend of -0.31 mm/day/decade (significant at the 90% confidence level) and $+0.38$ mm/day/decade (significant at the 95% confidence level) in the pre-MO period and the post-MO period, respectively (Fig. 1c).

Long-term variation of fronts in the pre-MO and post-MO periods

As a major component of the precipitation in the pre-rainy season^{34,35}, frontal precipitation is induced mainly by cold fronts and quasi-stationary fronts in the pre- and post-MO periods because of the seasonal cycle of background circulations^{16,36}. The location, intensity, and stationarity of the fronts affect the characteristics of precipitation variation, and quasi-stationary fronts usually trigger intense and persistent precipitation events. In this study, frontal variation is measured by an accumulated frontal activity (FA) index and a front stationarity (FS) index (see Methods for detailed definitions). The FA index reflects both the front intensity and the front frequency.

Consistently, the front indices over southern China also show an opposite long-term trend in the pre-MO and post-MO periods. During the pre-MO period, the FA over southern China displays a robust weakening trend and the fronts become less stationary (Fig. 2, Supplementary Fig. 3), consistent with the decreasing precipitation trend. The weakening trend in frontal activity is also reflected by weakened baroclinicity in the lower troposphere over southern China during the pre-MO period³⁶. As an indication of cold air intrusion from north, the weakening trend in FA also implies weaker forcing from higher latitudes. In contrast, during the post-MO period, the moderately enhanced FA and the prominently increasing trend in the FS index (more stationary) suggest that the fronts become stronger and more persistent, which is conducive to more extreme precipitation events (Fig. 2d). The above results demonstrate that the drying trend in the pre-MO period is associated with less frontal activity, while the wetting

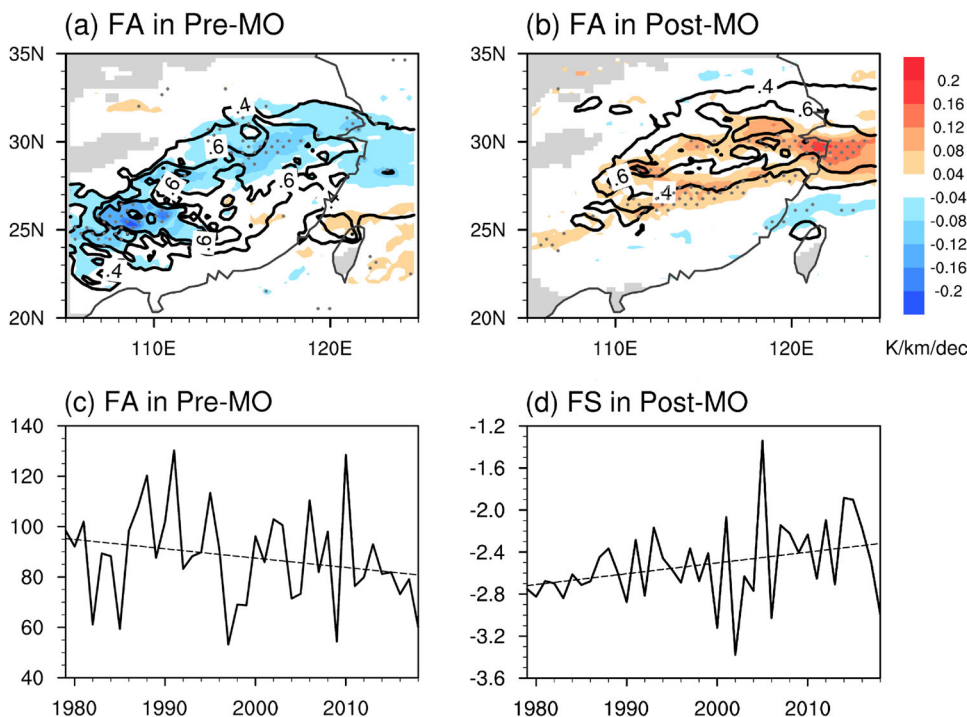


Fig. 2 Trends and variations in the characteristics of fronts. Trends of the accumulated frontal activity (FA) in **a** pre-MO and **b** post-MO periods during 1979–2018 (shading, K/km/decade). Contours show the corresponding climatology of each period (K/km). Time series of **c** FA index in the pre-MO period and **d** front stationarity (FS) index in the post-MO period over SC. Stippled areas in **a** and **b** are significant at the 0.05 level. Slanted straight lines in **c** and **d** represent the linear regression results, which are significant at the 0.1 and 0.05 levels, respectively.

trend in the post-MO period is related coherently to enhanced front stationarity.

The formation and variation of fronts over southern China are closely related to the southward intrusion of synoptic disturbances from the mid-latitudes^{35,37}. Based on case analyses in this study (Fig. 3), frequent southward intrusion of active mid-latitude synoptic disturbances favors the formation of fronts to induce precipitation, while the synoptic disturbances should be suppressed to some extent in order to maintain the stationarity of the fronts to produce intense precipitation. Note that during the pre-MO period (before the summer monsoon circulation establishes), the formation of fronts matters more for precipitation, while during the post-MO period, fronts readily form along the establishment of the summer monsoon circulation, and thus the stationarity of fronts accounts more for precipitation (Fig. 3; Supplementary Figure 3). During the study period, 1980 and 1998 had almost the largest amount of precipitation in southern China in the pre-MO and post-MO periods, respectively (see Fig. 1c). As shown in Fig. 3a, 2–8-day synoptic disturbances were active in the pre-MO period of 1980. The frequent formation of fronts (3 April, 18 April, and 3 May) was accompanied by southward intrusion of disturbances. Strong disturbances during 14–19 April pushed fronts farther southward and paused the precipitation over southern China. Therefore, the heavy precipitation in the pre-MO period of 1980 was caused by active frontal activity due to frequent intrusion of cold air. As shown in Fig. 3b, during the post-MO period of 1998 and after a front formed in mid-May, the relatively weak synoptic disturbances from the mid-latitudes helped maintain the persistence of the monsoonal front over southern China, producing a long-lasting precipitation event. The extreme precipitation episode began in late May along with a quasi-stationary front and fewer mid-latitude synoptic disturbances. Heavy floods occurred in the Yangtze River Valley in the

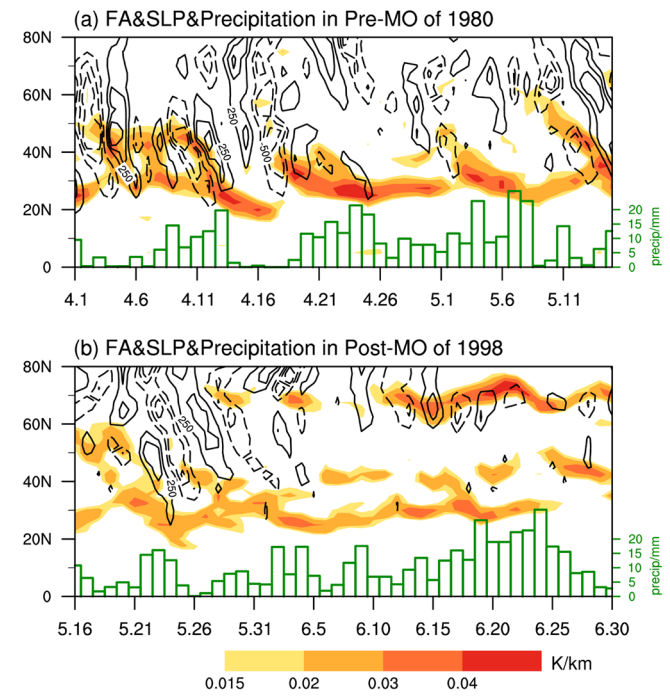


Fig. 3 Inter-connections among mid-latitude synoptic disturbances, fronts, and SC precipitation. Daily $|\frac{\partial \theta_e}{\partial p}|$ (shading, K/km) and 2–8-day filtered SLP (contours, Pa) averaged over 105–120°E and daily precipitation over SC (green bars, mm) in **a** the pre-MO period of 1980 and **b** the post-MO period of 1998. The fronts are indicated by shadings.

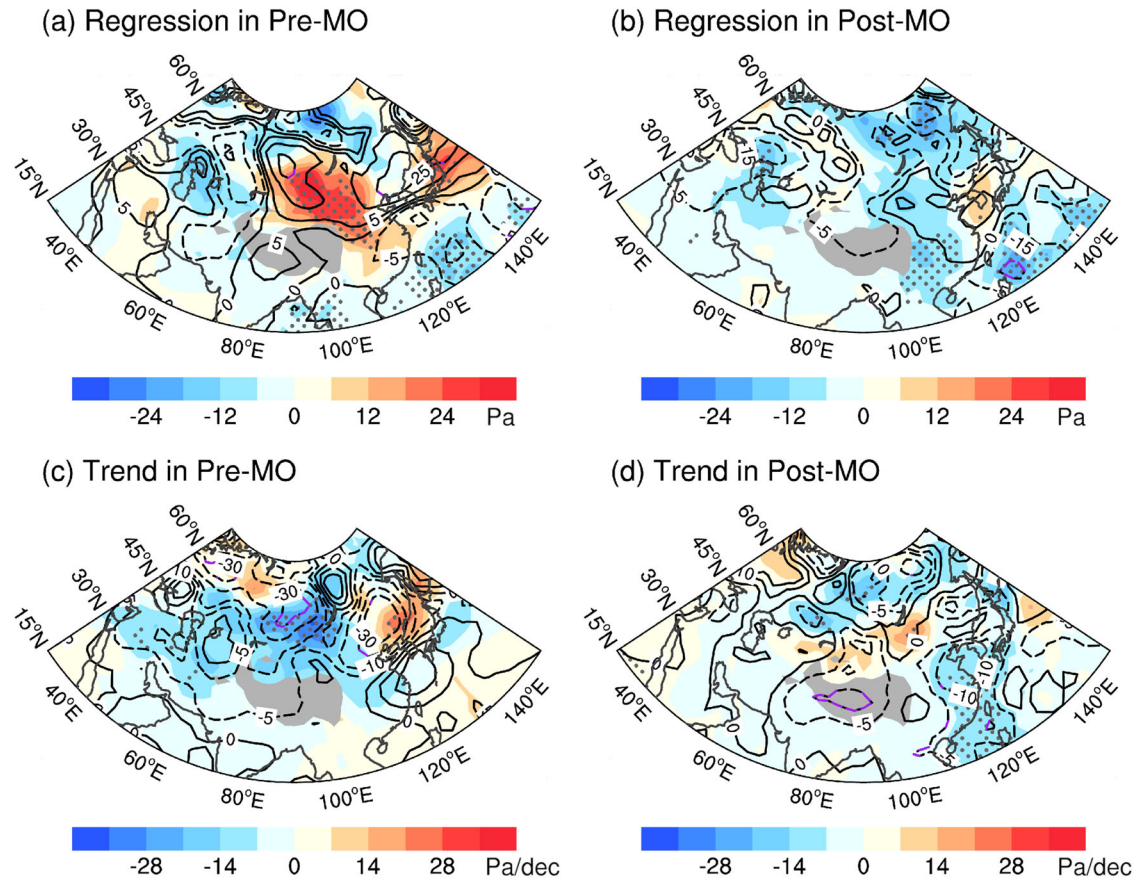


Fig. 4 Relationship between SC precipitation and mid-latitude synoptic disturbances. **a, b** Regressed root-mean-square (RMS) of 2–8-day filtered SLP (shading, Pa) and 500-hPa geopotential height (contours, m^2/s^2) against precipitation index over SC (see Fig. 1c) and **c, d** trends in RMS of 2–8-day filtered SLP (shading, Pa/decade) and 500-hPa geopotential height (contours, $\text{m}^2/\text{s}^2/\text{decade}$) in the (left) pre-MO and (right) post-MO periods. Stippled areas and purple contours are significant at the 0.05 level.

summer of 1998, which caused economic losses of about 40 billion USD³⁸.

In summary, frontal activity accounts more for the precipitation in the pre-MO period and exhibits a weakening trend, consistent with the drying trend of precipitation, while front stationarity acts as a major contributor to the precipitation in the post-MO period and shows an increasing trend (more stationary), consistent with the wetting trend of precipitation. Both the weakening of frontal activity and the strengthening of front stationarity can be modulated by the variation of synoptic disturbances from the mid-latitudes.

Impact of weakened synoptic disturbances in the mid-latitudes

The multi-year root-mean-square (RMS) of the 2–8-day filtered sea level pressure (SLP) regressed against the southern China precipitation index reveals a nearly inverse relationship over mid-latitude East Asia between the pre-MO and post-MO periods (Fig. 4). In the pre-MO period, enhanced precipitation over southern China is associated with stronger synoptic disturbances in Siberia and east of the Tibetan Plateau and suppressed synoptic eddies in the low latitudes over the western North Pacific (Fig. 4a). In contrast, more precipitation over southern China in the post-MO period is linked to suppressed synoptic disturbances over most of Eurasia including southern China (Fig. 4b). The above linkages are broadly similar when the regression analysis is repeated with 500-hPa geopotential height (contours in Fig. 4a, b). The above results indicate that the precipitation anomaly over southern China is associated with anomalous mid-latitude

synoptic disturbances with an equivalent barotropic structure, but the sign is reversed in the pre-MO and post-MO periods.

One may wonder whether the long-term variation of synoptic disturbances could explain the long-term variation of southern China precipitation in the pre-MO and post-MO periods. As shown in Fig. 4c, the RMS of the 2–8-day filtered SLP has a strongly negative trend over Siberia. Compared to the regression map in Fig. 4a, the negative trend shows that the synoptic disturbances from the mid-latitudes are suppressed and inhibit southern China precipitation in the pre-MO period. Similarly, the RMS of the 2–8-day filtered 500-hPa geopotential height has weakening trends over most of Eurasia, with two centers over Siberia and near the Sea of Okhotsk. In the post-MO period (Fig. 4d), the RMS of the 2–8-day filtered SLP over the majority of East Asia exhibits a decreasing trend, especially over eastern China and its adjacent oceans, while the RMS of the 500-hPa geopotential height also shows a decreasing trend over the Tibetan Plateau. This feature implies that the weakening of large-scale synoptic disturbances in the mid-latitudes likely contributes to the increasing trend of southern China precipitation in the post-MO period. Overall, the reversed precipitation trend in the pre-MO and post-MO periods is attributed to the persistent weakening trend of synoptic disturbances over the mid-latitudes. The causality between the trend of precipitation and the trend of mid-latitude synoptic disturbances can be interpreted by the frontal variation as discussed previously. The weakening of synoptic forcing from the mid-latitudes results in less frontal activity (Supplementary Fig. 4) and reduced frontal precipitation in the pre-MO period, and

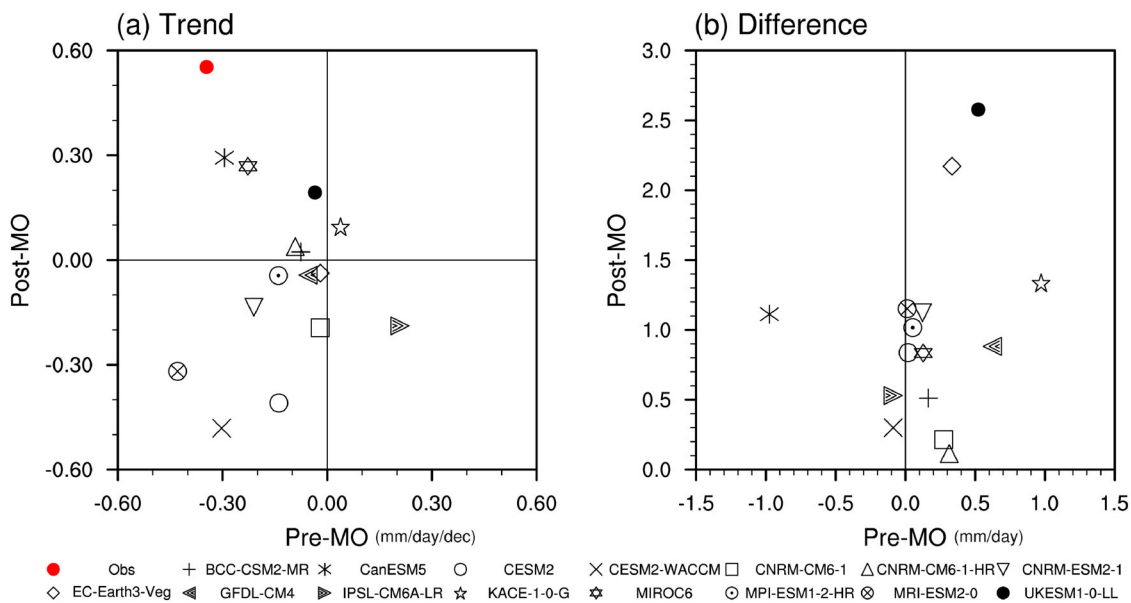


Fig. 5 Precipitation trends and projected precipitation changes in CMIP6 models. a Precipitation trends (mm/day/decade) over SC in the pre-MO and post-MO periods during 1979–2014 from 15 CMIP6 models (black markers), according to the specific onset time of each model. Model names are listed at the bottom of the plot. The solid red dot is observed trends in 1979–2014. **b** Differences in precipitation (mm/day) over SC between the historical (1979–2014) and SSP5-85 (2065–2100) (2065–2100 minus 1979–2014) runs of the 15 CMIP6 models.

more quasi-stationary fronts (Supplementary Fig. 4) and persistent heavy precipitation in the post-MO period.

Future projection of precipitation over southern China

To further investigate whether the opposite precipitation trend is a climate change signal or part of interdecadal variation, we analyze the outputs from 15 CMIP6 models (see details in Methods). In the historical runs, five models are able to reproduce the opposite precipitation trends over southern China in the pre-MO and post-MO periods during 1979–2014, with two models—CanESM5 and MIROC6—performing better, although the simulated trends are weaker than the observed in both periods (weaker drying/wetting in the pre-MO/post-MO period) (Fig. 5a). It is a challenge for most of the models to simulate the observed opposite trend of precipitation over southern China. Among the three capable models, CanESM5 has the best performance in reproducing the opposite precipitation trend and simulating the relationship between the precipitation over southern China and synoptic disturbances, although some discrepancies from observations still exist (Supplementary Fig. 6). The model's capability might result from its good performance in simulating circulations in the mid- to high latitudes³⁹. Apparently, the long-term trends of monsoonal precipitation over southern China can be well simulated only when the model can reproduce the variation of synoptic disturbances in the mid-latitudes. Interestingly, the precipitation projection by CanESM5 in the Shared Socioeconomic Pathway (SSP) 5-85 scenario (Fig. 5b) also shows a drying trend in the pre-MO period and a wetting trend in the post-MO period. This is different from most models, which show a wetting trend in both the pre-MO and post-MO periods. It should also be noted that MIROC6 and UKESM1-0-LL simulate a larger wetting trend in the post-MO period than in the pre-MO period.

In CanESM5, the future pre-MO precipitation projection over East Asia shows a “wetter north and drier south” pattern (Fig. 6a). The “wetter north” precipitation is associated with stronger synoptic disturbances extending northeastward from northern China to the Sea of Okhotsk (Fig. 6c). The “drier south” precipitation is related to

suppressed synoptic disturbances (at both SLP and 500 hPa) over southern China and north and west of the Tibetan Plateau (Fig. 6c). It appears that the weakening trend of synoptic disturbances contributes to the drying trend over southern China in the pre-MO period. On the other hand, the future post-MO projection shows a wetting trend across East Asia, with one belt elongating north-eastward from southern China to southern Japan and another belt extending from the Tibetan Plateau to the Korean Peninsula (Fig. 6b). The southern belt resembles the typical pattern of the “Meiyu-Baiu” front, implying an enhancement of quasi-stationary frontal precipitation in the future^{40,41}. Synoptic disturbances in the post-MO period exhibit a weakening trend across the Asian continent, with a center over Siberia (Fig. 6d). The weakened synoptic disturbances favor stationarity of monsoonal fronts, such as the Meiyu-Baiu front, and potentially trigger more heavy precipitation and flooding in the post-MO period⁴², consistent with results of Ha et al.⁴³.

Therefore, the opposite precipitation trends over southern China before and after the SCSSM onset are likely associated with the climate change during recent decades although internal decadal-scale variability might also have non-negligible contributions. These trends are related to the weakening trend of mid-latitude synoptic disturbances over East Asia.

DISCUSSION

Although global subtropical precipitation shows a declining trend under global warming, precipitation over southern China, a subtropical monsoon region, presents complex variation and strong seasonality. In this study, we reveal that southern China precipitation displays a significant drying trend in the pre-MO period and a significant wetting trend in the post-MO period under global climate change in recent decades. In other words, in southern China the hydroclimatic transition from spring to summer will be more abrupt and the precipitation will be more concentrated in the post-MO period.

This study examines the impact of mid-latitude synoptic disturbances on the reversed precipitation trend. The southern China pre-MO precipitation is usually induced by the southward

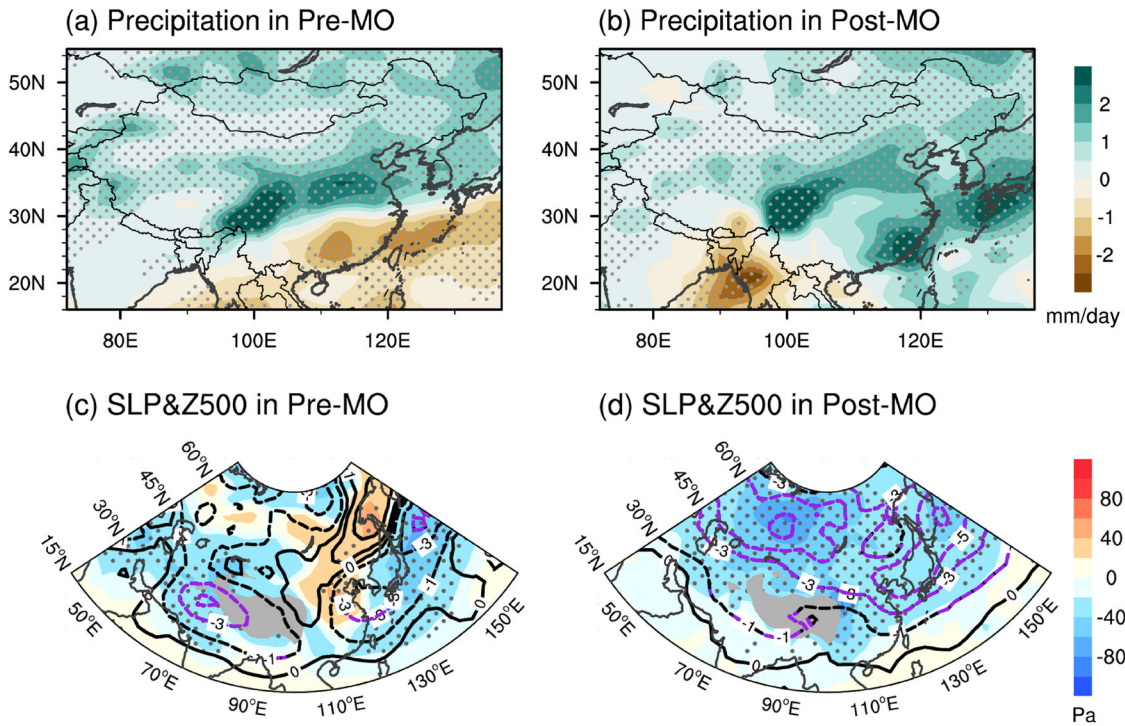


Fig. 6 Projected changes in precipitation and synoptic disturbances in CanESM5. Differences between the historical run (1979–2014) and the SSP5-85 run (2065–2100) of CanESM5 in **a, b** precipitation (mm/day) and **c, d** the RMS of 2–8-day filtered SLP (shading, Pa) and 500-hPa geopotential height (contours, m) in (left) pre-MO and (right) post-MO periods. Stippled areas in **a** and **b** are significant at the 0.01 level. Dotted areas and purple contours in **c** and **d** are significant at the 0.05 level.

intrusion of mid-latitude cold fronts due to active mid-latitude synoptic disturbances, while the southern China post-MO precipitation is enhanced by quasi-stationary fronts supported by moderate and even suppressed mid-latitude synoptic disturbances. The opposite precipitation trends in the two periods can be explained by the trend of frontal activity over East Asia. In general, mid-latitude synoptic disturbances are suppressed under global warming. This reduces the southward migration of frontal activity to southern China in the pre-MO period and promotes more quasi-stationary fronts over southern China in the post-MO period. Hence, the suppressed mid-latitude synoptic disturbances could explain both the drying trend in the pre-MO period and the wetting trend in the post-MO period.

Climate models should capture the long-term weakening trend of synoptic disturbances in order to reproduce the opposite precipitation trend in the pre-MO and post-MO periods. However, this is a challenge for most models, and only 3 out of 15 CMIP6 models are capable to well simulate these trends in the present climate. CanESM5 has the best performance in reproducing the opposite precipitation trend over southern China in the pre-MO and post-MO periods. The CanESM5 future projection in the SSP5-85 scenario also shows a similar reversed precipitation trend. Specifically, the projection in the pre-MO period shows a drying trend over southern China and the western North Pacific, associated with a weakening trend of synoptic disturbances north and west of the Tibetan Plateau. The projection in the post-MO period shows a wetting trend along the typical “Meiyu-Baiu” front, which extends from southern China to southern Japan. This is related to a weakening trend of synoptic activity in the entire East Asian continent with a center over Siberia, which would favor the stationarity of the Meiyu-Baiu front. The frequency of extreme precipitation events would probably increase in the post-MO period, which might cause a larger socioeconomic impact. Future work should improve the simulation of mid-latitude synoptic disturbances in order to better simulate the long-term variation of

southern China precipitation in both pre-MO and post-MO periods. Note that this study does not discuss the impact of disturbances from tropical regions, for instance synoptic or intra-seasonal oscillations, which can also modulate the precipitation trend over southern China. Relative contributions of the synoptic forcing from mid-latitudes and tropical areas in the pre-MO and post-MO periods also need further investigation.

Besides the mid-latitude forcings investigated in this study, the drying trend in the pre-MO period coincides with a positive-to-negative phase shift in the Pacific Decadal Oscillation in April-May, while the wetting trend in the post-MO period occurs with a positive-phase tendency of the Atlantic Multidecadal Oscillation in May-June (see Supplementary Note 3 for detail). Like the mechanism proposed by Zhu et al.²⁶, the tropical La Niña-like decadal SST anomalies in spring and warming in the Indian Ocean in summer contribute to the spring drying and summer wetting over southern China. The observed opposite precipitation trends are thus robust with the non-negligible modulations from interdecadal internal variation.

METHODS

Observation dataset

The gridded precipitation data have a horizontal resolution of $0.5^\circ \times 0.5^\circ$ and are derived from more than 2000 gauge stations of the Chinese Meteorological Administration (CMA) with high quality control. Daily atmospheric variables, including air temperature, specific humidity, sea level pressure, and geopotential height, are derived from the 6-hourly (00, 06, 12, and 18 UTC) archives of the ERA-5 (fifth generation of the European Centre for Medium-Range Weather Forecasts) reanalysis dataset (C3S 2017)⁴⁴.

CMIP6 model dataset

We examine the outputs of 15 models from CMIP6 (phase 6 of the Coupled Model Intercomparison Project; Table 1). Historical runs for the period 1979–2014 are the present-day simulation, while future projections for the

Table 1. Descriptions of 15 CMIP6 models employed in the study.

Model acronym	Institute	Atmosphere resolution (lat × lon)
BCC_CSM2-MR	Beijing Climate Center, China Meteorologica	160 × 320
CanESM5	Canadian Centre for Climate Modeling and Analysis (CCCma)	64 × 128
CESM2	National Center for Atmospheric Research (NCAR)	192 × 288
CESM2(WACCM)		192 × 288
CNRM-CM6.1	Centre National de Recherches Meteorologiques/Centre European de Recherche et Formation Avancees en Calcul Scientifique (CNRM/CERFACS)	128 × 256
CNRM-CM6-1-HR		128 × 256
CNRM-ESM2.1		128 × 256
EC-EARTH3-Veg	European Consortium (EC)	256 × 512
GFDL CM4	Geophysical Fluid Dynamics Laboratory (NOAA GFDL)	180 × 288
IPSL-CM6A-LR	Institute Pierre-Simon Laplace (IPSL)	143 × 144
KACE-1.0-G	National Institute of Meteorological Sciences/Korea Meteorological Administration (NIMS-KMA)	144 × 192
MIROC6	Atmosphere and Ocean Research Institute (University of Tokyo), National Institute for Environmental Studies, and Japan Agency for Marine-Earth Science and Technology (MIROC)	128 × 256
MPI-ESM1.2-HR	Max Planck Institute for Meteorology (MPI-M)	192 × 384
MRI-ESM2.0	Meteorological Research Institute (MRI)	160 × 320
UKESM1.0-LL	Natural Environment Research Council and the Met Office Hadley Centre	144 × 192

period 2065–2100 under the Shared Socioeconomic Pathway 5-8.5 (SSP5-8.5) are used to assess the climate change impact by comparison to the present-day simulation. The SSP5-8.5 scenario is an updated version of the representative concentration pathway 8.5 (RCP8.5) of CMIP5, assuming that radiative forcing will stabilize at about 8.5 W/m² after 2100 and will cause global warming of about 4.3 °C by 2100 relative to the pre-industrial period (1850).

Precipitation index

The precipitation index in the pre-MO and post-MO periods is defined as the weighted areal-mean precipitation over southern China (20–28°N/105–120°E) for the period 1 April–15 May and the period 16 May–30 June.

Front indices

The derivation of front indices from the daily temperature and specific humidity at 850 hPa is briefly described below, with details in Li et al.⁴⁵. First, we compute the equivalent potential temperature θ_e at 850 hPa following the method of Bolton⁴⁶. Second, following Ding and Chan¹⁵, we define fronts using the meridional gradient of equivalent potential temperature, $\frac{\partial \theta_e}{\partial y}$. Frontal areas are first detected by a threshold of $\frac{\partial \theta_e}{\partial y} \leq -0.04K/km$ with the zonal extension larger than the meridional extension (Supplementary Fig. 5). Thresholds of the frontal area are set as a 20-degree square and an 18-degree square for the pre-MO and post-MO periods, respectively, due to the different climate background of the two periods. When a day satisfies the threshold, it is detected as a frontal day. Third, once frontal days are detected, the daily frontal activity index is defined as the weighted areal sum of $|\frac{\partial \theta_e}{\partial y}|$ over the area satisfying the threshold, and the daily frontal central latitude is defined as the weighted areal mean latitude over the frontal area. Fourth, the accumulated frontal activity index (FA) is defined as the sum of the daily frontal activity index during the pre-MO period and the post-MO period for a year. The front stationarity index (FS) is defined as the reverse sign of the standard deviation of the daily frontal central latitude during the pre-MO period and the post-MO period for a year.

DATA AVAILABILITY

The ERA5 and CMIP6 datasets are publicly available online (<https://cds.climate.copernicus.eu/#/search?text=ERA5&type=dataset> and <https://esgf-node.llnl.gov/projects/cmip6/>). The gridded precipitation observation dataset is available from the National Climate Center, China Meteorological Administration (<http://data.cma.cn/>).

CODE AVAILABILITY

The codes used to produce the figures and to compute the front indices are available from the corresponding author on request.

Received: 14 September 2021; Accepted: 5 April 2022;
Published online: 17 May 2022

REFERENCES

- Held, I. M. & Soden, B. J. Robust responses of the hydrological cycle to global warming. *J. Clim.* **19**, 5686–5699 (2006).
- He, J. & Soden, B. J. A re-examination of the projected subtropical precipitation decline. *Nat. Clim. Change* **7**, 53–57 (2017).
- Zappa, G., Ceppi, P. & Shepherd, T. G. Time-evolving sea-surface warming patterns modulate the climate change response of subtropical precipitation over land. *Proc. Natl Acad. Sci.* **117**, 4539–4545 (2020).
- Norris, J., Chen, G. & Li, C. Dynamic amplification of subtropical extreme precipitation in a warming climate. *Geophys. Res. Lett.* **47**, e2020GL087200 (2020).
- Chen, Z. et al. Global land monsoon precipitation changes in CMIP6 projections. *Geophys. Res. Lett.* **47**, e2019GL086902 (2020).
- Song, L. Overview of meteorological disasters in Guangdong. In: *Yearbook of Meteorological Disasters in China*, China Meteorological Administration, 144–p146 (2013).
- Zhu, Q. & He, J. On features of the upper circulations in the establishment of the Asian monsoon in 1979 and its medium-range oscillations. *J. Trop. Meteorol.* **1**, 9–18 (1985).
- Ding, Y. *The Asian monsoon*, 76–83 (China Meteorological Press, 1994).
- Ting, M. Maintenance of northern summer stationary waves in a GCM. *J. Atmos. Sci.* **51**, 3286–3308 (1994).
- Chen, P., Hoerling, M. & Dole, R. The origin of the subtropical anticyclones. *J. Atmos. Sci.* **58**, 1827–1835 (2001).
- Rodwell, M. J. & Hoskins, B. J. Subtropical anticyclones and summer monsoons. *J. Clim.* **14**, 3192–3211 (2001).
- Chen, T. Characteristics of summer stationary waves in the Northern Hemisphere. *J. Clim.* **23**, 4489–4507 (2010).
- Shaw, T. & Voigt, A. Tug of war on summertime circulation between radiative forcing and sea surface warming. *Nat. Geosci.* **8**, 560–566 (2015).
- Lau, K.-M. & Yang, S. Climatology and interannual variability of the Southeast Asian summer monsoon. *Adv. Atmos. Sci.* **14**, 141–162 (1997).
- Ding, Y. & Chan, J. C. L. The East Asian summer monsoon: an overview. *Meteorol. Atmos. Phys.* **89**, 117–142 (2005).
- Zheng, B., Liang, J., Lin, A., Li, C. & Gu, D. Frontal rain and summer monsoon rain during pre-rainy season in South China. Part 1: determination of the division date. *Chin. J. Atmos. Sci.* **30**, 1207–1216 (2006).

17. LinHo, L. H., Huang, X. & Lau, N. C. Winter-to-spring transition in East Asia: a planetary-scale perspective of the south China spring rain onset. *J. Clim.* **21**, 3081–3096 (2008).
18. Li, R. C. Y. & Zhou, W. Multiscale control of summertime persistent heavy precipitation events over South China in association with synoptic, intraseasonal, and low-frequency background. *Clim. Dyn.* **45**, 1043–1057 (2015).
19. Sampe, T. & Xie, S. P. Large-scale dynamics of the Meiyu–Baiu rainband: environmental forcing by the westerly jet. *J. Clim.* **23**, 113–134 (2010).
20. Zhu, Z., He, J. & Qi, L. Seasonal transition of East Asian subtropical monsoon and its possible mechanism. *J. Trop. Meteorol.* **18**, 305–313 (2012).
21. Kwon, M., Jhun, J.-G. & Ha, K.-J. Decadal change in East Asian summer monsoon circulation in the mid-1990s. *Geophys. Res. Lett.* **34**, L21706 (2007).
22. Wang, B. et al. Multiscale climate variability of the South China Sea monsoon: a review. *Dyn. Atmos. Oceans* **47**, 15–37 (2009).
23. Li, J., Wu, Z., Jiang, Z. & He, J. Can global warming strengthen the East Asian summer monsoon? *J. Clim.* **23**, 6696–6705 (2010).
24. Kajikawa, Y. & Wang, B. Interdecadal change of the South China Sea summer monsoon onset. *J. Clim.* **25**, 3207–3218 (2012).
25. Li, Y. et al. Multi-scale temporal-spatial variability of the East Asian summer monsoon frontal system: observation versus its representation in the GFDL HIRAM. *Clim. Dyn.* **52**, 6787–6798 (2019).
26. Zhu, Z., Li, T. & He, J. Out-of-phase relationship between boreal spring and summer decadal rainfall changes in southern China. *J. Clim.* **27**, 1083–1099 (2014).
27. Coumou, D., Lehmann, J. & Beckmann, J. The weakening summer circulation in the Northern Hemisphere mid-latitudes. *Science* **348**, 324–327 (2015).
28. Zhao, S., Deng, Y. & Li, W. A nonmodal instability perspective of the declining northern midlatitude synoptic variability in boreal summer. *J. Clim.* **33**, 1177–1192 (2020).
29. Pfleiderer, P. & Coumou, D. Quantification of temperature persistence over the Northern Hemisphere land-area. *Clim. Dyn.* **51**, 627–637 (2018).
30. Weaver, S., Kumar, A. & Chen, M. Climate extremes: patterns and mechanisms. In: *Geophysical Monograph 1st edn* (eds Simon Wang, S.-Y. et al.) 105–114 (Wiley, New York, 2017).
31. Coumou, D., Di Capua, G., Vavrus, S., Wang, L. & Wang, S. The influence of Arctic amplification on mid-latitude summer circulation. *Nat. Commun.* **9**, 2959 (2018).
32. Lehmann, J. & Coumou, D. The influence of mid-latitude storm tracks on hot, cold, dry and wet extremes. *Sci. Rep.* **5**, 17491 (2015).
33. Cohen, J. et al. Recent Arctic amplification and extreme mid-latitude weather. *Nat. Geosci.* **7**, 627–637 (2014).
34. Chen, G. T. J. Research on the phenomena of Meiyu during the past quarter century: an overview. In: *The East Asian Monsoon* (ed. Chang CP) 357–403 (World Scientific, 2004).
35. Ninomiya, K. Large- and mesoscale features of Meiyu–Baiu front associated with intense rainfalls. In: *East Asian Monsoon* (ed. Chang CP) 404–435 (World Scientific, 2004).
36. Luo, X. & Zhang, Y. Interdecadal change in the seasonality of rainfall variation in South China. *Theor. Appl. Climatol.* **119**, 1–11 (2015).
37. Wang, Y. Effects of blocking anticyclones in Eurasia in the rainy season Meiyu/Baiu season. *J. Meteorol. Soc. Jpn.* **70**, 929–950 (1992).
38. Lu, R. Anomalies in the tropics associated with the heavy rainfall in East Asia during the summer of 1998. *Adv. At. Sci.* **17**, 205–220 (2000).
39. Li, Y., Leung, L. R., Xiao, Z., Wei, M. & Li, Q. Interdecadal connection between Arctic temperature and summer precipitation over the Yangtze River Valley in the CMIP5 historical simulations. *J. Clim.* **26**, 7464–7488 (2013).
40. Ding, Y., Liang, P., Liu, Y. & Zhang, Y. Multiscale variability of Meiyu and its prediction: a new review. *J. Geophys. Res. Atmos.* **125**, e2019JD031496 (2020).
41. Li, Y. et al. Projected changes in the characteristics of the East Asian summer monsoonal front and their impacts on the regional precipitation. *Clim. Dyn.* **56**, 4013–4026 (2021).
42. Chiang, J. C. H., Fischer, J., Kong, W. & Herman, M. J. Intensification of the pre-Meiyu rainband in the late 21st century. *Geophys. Res. Lett.* **46**, 7536–7545 (2019).
43. Ha, K.-J., Moon, S., Timmermann, A. & Kim, D. Future changes of summer monsoon characteristics and evaporative demand over Asia in CMIP6 simulations. *Geophys. Res. Lett.* **47**, e2020GL087492 (2020).
44. Copernicus Climate Change Service (C3S): ERA5: Fifth generation of ECMWF atmospheric reanalyses of the global climate. Copernicus Climate Change Service Climate Data Store (CDS), <https://cds.climate.copernicus.eu/cdsapp#!/home> (2017).
45. Li, Y., Deng, Y., Yang, S. & Zhang, H. Multi-scale temporospatial variability of the East Asian Meiyu–Baiu fronts—Characterization with a suite of new objective indices. *Clim. Dyn.* **51**, 1659–1670 (2018).
46. Bolton, D. The computation of equivalent potential temperature. *Mon. Weather Rev.* **108**, 1046–1053 (1980).

ACKNOWLEDGEMENTS

This study is supported by the National Natural Science Foundation of China (Grants 42105058, 42088101, 42120104001, 41905050, 42075028, and 4210050324). Y.D. is supported in part by the U.S. National Science Foundation (NSF) through Grant AGS-2032532 and by the U.S. National Oceanic and Atmospheric Administration (NOAA) through Grant NA20OAR4310380. H.-N.C. is supported by the Guangdong Basic and Applied Basic Research Fund (Grants 2020B030103004 and 2021A1515012419). W.Z. is supported by the Hong Kong RGC General Research Fund 11300920, and a project of the Center for Ocean Research in Hong Kong and Macau (CORE).

AUTHOR CONTRIBUTIONS

Y.L., Y.D., and W.Z. designed the study. Y.L. and H.C. performed the research and analyzed the data. Y.L., Y.D., H.C., S.Y., and H.Z. wrote the manuscript, and all authors contributed to the discussion of results and the revision of the manuscript.

COMPETING INTERESTS

The authors declare no competing interests.

ADDITIONAL INFORMATION

Supplementary information The online version contains supplementary material available at <https://doi.org/10.1038/s41612-022-00259-1>.

Correspondence and requests for materials should be addressed to Yana Li or Wen Zhou.

Reprints and permission information is available at <http://www.nature.com/reprints>

Publisher's note Springer Nature remains neutral with regard to jurisdictional claims in published maps and institutional affiliations.



Open Access This article is licensed under a Creative Commons Attribution 4.0 International License, which permits use, sharing, adaptation, distribution and reproduction in any medium or format, as long as you give appropriate credit to the original author(s) and the source, provide a link to the Creative Commons license, and indicate if changes were made. The images or other third party material in this article are included in the article's Creative Commons license, unless indicated otherwise in a credit line to the material. If material is not included in the article's Creative Commons license and your intended use is not permitted by statutory regulation or exceeds the permitted use, you will need to obtain permission directly from the copyright holder. To view a copy of this license, visit <http://creativecommons.org/licenses/by/4.0/>.

© The Author(s) 2022